Fusion Peptide from Influenza Hemagglutinin Increases Membrane Surface Order: An Electron-Spin Resonance Study

Mingtao Ge and Jack H. Freed*
National Biomedical Center for Advanced ESR Technology, Department of Chemistry and Chemical Biology, Cornell University, Ithaca, New York 15853

ABSTRACT A spin-labeling study of interactions of a fusion peptide from the hemagglutinin of the influenza virus, wt20, and a fusion-inactive mutant ΔG1 with dimyristoylphosphatidylcholine (DMPC) and 1-palmitoyl-2-oleoyl-phosphatdylcholine bilayers was performed. We found that upon binding of wt20, the ordering of headgroups and the ordering of acyl chains near the headgroup increased significantly, in a manner consistent with a cooperative phenomenon. However, changes in the order at the end of the acyl chains were negligible. The ordering effect of wt20 on the headgroup was much stronger at pH 5 than at pH 7. No effect of ΔG1 binding on the order of bilayers was evident. We also found that 1-palmitoyl-2-hydroxyl phosphatidylcholine, a membrane-fusion inhibitor, decreased the ordering of DMPC headgroups, whereas arachidonic acid, a membrane-fusion promoter, increased the ordering of DMPC headgroups. These results suggest that increases in headgroup ordering may be important for membrane fusion. We propose that upon binding of wt20, which is known to affect only the outer leaflet of the bilayer, this outer leaflet becomes more ordered, and thus more solid-like. Then the coupling between the hardened outer leaflet and the softer inner leaflet generates bending stresses in the bilayer, which tend to increase the negative curvature of the bilayer. We suggest that the increased ordering in the headgroup region enhances dipolar interactions and lowers electrostatic energy, which may provide an energy source for membrane fusion. Possible roles of bending stresses in promoting membrane fusion are discussed.

INTRODUCTION

Viral membrane fusion is mediated by glycoprotein (a fusion protein) (1,2). Activated by binding to host-cell receptors or by a pH change, the N-terminal segment of glycoprotein, the so-called fusion peptide, which usually consists of 20–30 amino-acid residues, becomes exposed and inserts into the target membrane. Insertion of the fusion peptide is thought to destabilize the structure of the target bilayer, initiating membrane fusion. The membrane-destabilizing effects of the fusion peptide are manifested by lipid mixing, content leakage, swelling, and lysis of vesicles (3–9).

Various biophysical and spectroscopic techniques, along with computational methods, were used to study the membrane structure of the fusion peptide and interactions of fusion peptide with lipid bilayers, in an effort to understand how the bilayer structure is disturbed by the fusion peptide, in promoting viral membrane fusion (4,10–17). One focus of these studies was to investigate whether fusion peptide increases or decreases bilayer ordering (18–30). Studies of the mutation of fusion peptide from the hemagglutinin (HA) of influenza virus showed that fusion peptides that are more fusogenic have a greater ordering effect on bilayers than those that are less fusogenic (28,29). However, the results of molecular dynamics studies showed that both a wild-type HA2 fusion peptide (wt20) and a more fusion active analog (E5) disordered the bilayers (20–22). It remains unclear how changes in membrane ordering modify the bilayer structure, thereby affecting membrane fusion.

In previous studies, we measured the ordering in the headgroup and acyl chain regions in both model and biomembranes, using electron-spin resonance (ESR) labeling (31–35) combined with nonlinear least-squares (NLLS) spectral fitting (36). These measurements provided valuable insights into the nature of the interactions of proteins with model membranes and the domain structure of biological membranes. Here, we observed distinct changes in the ordering of dimyristoylphosphatidylcholine (DMPC) and 1-palmitoyl-2-oleoyl-phosphatdylcholine (POPC) bilayers upon the binding of wt20 versus ΔG1 (deletion of the N-terminal glycine of wt20) (37). We found that: 1), the binding of wt20 to DMPC and POPC bilayers mainly increases the ordering in the headgroup region of the bilayers; 2), the binding of wt20 to the phosphatidylcholine (PC) bilayers shows a cooperative characteristic; 3) the headgroup-ordering effect of wt20 is pH-dependent; and 4), the binding of ΔG1 has no effect on lipid ordering. The significance of this increased ordering of headgroups is discussed in terms of its effect on enhancing bilayer negative curvature, which may promote membrane fusion.

MATERIALS AND METHODS

Materials and sample preparation

The lipids DMPC, POPC, and 1-palmitoyl-2-hydroxy phosphatidylcholine (lysoPC), and two chain spin labels 5PC and 14PC, and a headgroup spin label dipalmitoylphospatidyl-tempo-choine (DPPTC) were purchased from

Submitted January 7, 2009, and accepted for publication April 6, 2009.

*Correspondence: jhf@ccmr.cornell.edu

Editor: David D. Thomas.

0006-3495/09/06/4925/10 $2.00

doi: 10.1016/j.bpj.2009.04.015

Avanti (Alabaster, AL). Another heagroup spin label, 4-O-(1,2-dipalmitoyl-*sn*-glycero-3-phospho)-tempo (DPP-Tempo), was custom-synthesized by Nutrimed Biotech (Ithaca, NY). Tempo is an abbreviation for 2,2,6,6-tetramethyl-piperidine-1-oxy. The chemical structures of DPPTC and DPP-Tempo are depicted in Fig. 1. Arachidonic acid (AA) was purchased from Sigma-Aldrich (St. Louis, MO). The fusion peptide of HA2 from influenza virus (strain X31), wt20, and the mutant ΔG1 were synthesized by SynBio-Sci Co. (Livermore, CA):

wt20 : GLFGAIAGFIENGWEGMIDG

ΔG1 : LFGAIAGFIENGWEGMIDG

Measured stock solutions of DMPC or POPC (in chloroform) and the spin label (in chloroform) were mixed. The concentration of spin label was 0.5 mol % of the lipids. The solvent was evaporated by N_2 flow, and the sample was evacuated with a mechanical pump overnight to remove traces of solvent. Each sample (1 mg) was hydrated in 1 mL of a pH 5 buffer (5 mM HEPES, 5 mM MES, 5 mM sodium nitrate, and 10 mM NaCl), and also in 1 mL of a pH 7 buffer (50 mM Tris, 10 mM NaCl, and 0.1 mM EDTA) at room temperature overnight. Stock solutions of wt20 or ΔG1 (1 mM in DMSO, stored at 4°C), as measured using a Hamilton syringe, were added to the hydrated DMPC and POPC dispersions. After 1 min of vortexing, the dispersion was spun in a desktop centrifuge to produce a pellet, which was transferred to a quartz capillary tube for ESR measurement shortly afterward. These dispersions of multilamellar vesicle (MLV) were used to provide the needed ESR signal/noise sensitivity. Previous studies of the effects of fusion peptide on the membrane structure using MLV include those of lipid interactions of fusion peptides from HIV (19) and canine distemper virus (26).

ESR spectroscopy and nonlinear least-squares fit of ESR spectra

The ESR spectra were obtained on an EMX ESR spectrometer (Bruker Instruments, Billerica, MA) at a frequency of 9.55 GHz, equipped with a Varian (Palo Alto, CA) temperature-control unit with an absolute temperature accuracy of ±0.3°C.

The ESR spectra were analyzed using the NLLS fitting program (36), based on the stochastic Liouville equation (38,39). The rotational diffusion of the nitroxide radical in spin labels can be described as a restricted wobbling motion, characterized by two sets of parameters obtained from the spectral analysis. The first set consists of $R_\perp$ and $R_\parallel$, which are, respectively, the rates of rotation of the nitroxide radical around a molecular axis perpendicular and parallel to the preferential orienting axis of the acyl chain (or of the headgroup) to which the nitroxide radical is attached. The second set, S_0 and S_2, are the ordering tensor parameters. S_0 represents the average angular amplitude of the wobbling in the membrane. Upon wt20 binding, variations of S_0 reveal important changes in bilayer structure of relevance to this study, and thus the significance of S_0 will be further detailed in the Discussion. S_2 is a measure of the molecular nonaxiality of the wobbling motion. It was found to be much smaller than S_0, with much less sensitivity to wt20 binding.

The "microscopically ordered but macroscopically disordered" (MOMD) model (40) was used in spectral simulations. This was based on the structural characteristics of lipid vesicles, which are locally ordered (oriented) but globally disordered (randomly distributed). The MOMD model is included in the NLLS fitting program.

The hyperfine tensors and g-tensor values used in this study were determined from NLLS analysis of rigid limit spectra. They are given in Table S0 of the Supporting Material. We found that the addition of wt20 decreased the values of the z component of the A-tensor, A_{zz}, of DPP-Tempo and DPPTC in DMPC and POPC slightly, but by <0.5 G, and the addition of ΔG1 had no effect on A_{zz}. The incorporation of 10 mol % of lyso-PC or 10 mol % of AA had a slight effect on the value of A_{zz} of DPP-Tempo. The estimated error from the NLLS fit for the spectra was ±0.01 for the S_0 of 5PC and 14PC, ±0.006 for the S_0 of DPP-Tempo and DPPTC, ±5% for the $R_\perp$ of all spin labels, ±20% for the $R_\parallel$ of DPP-tempo and DPPTC, and ±50% for the $R_\parallel$ of 5PC and 14PC.

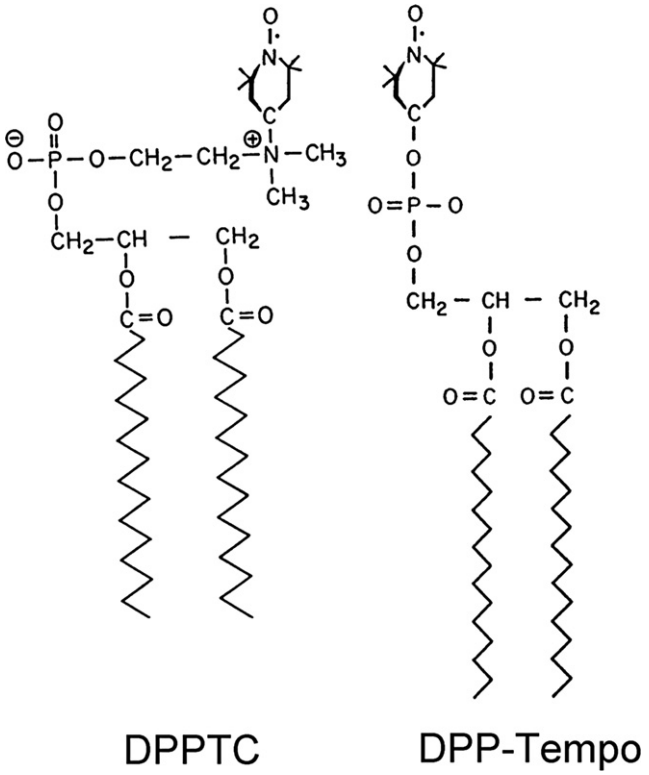

FIGURE 1 Chemical structures of spin labels DPPTC and DPP-Tempo.

RESULTS

The binding of wt20 and ΔG1 to DMPC and POPC was investigated at pH 5 and pH 7, using the headgroup spin label DPPTC (Fig. 1). The order parameter S_0 of DPPTC in DMPC versus the concentration of wt20 (*solid line*) and ΔG1 (*dashed line*) at 25°C and 37°C is plotted in Fig. 2. At pH 5 and 25°C in the range of molar concentration of wt20 (molar ratio of wt20/DMPC) from 0 to $<1.5 \times 10^{-3}$ (0 to 1/700), S_0 increases only slightly, going from 0.54 (pure DMPC) to 0.55. From a 1.5 to 1.7×10^{-3} (1/700 to 1/600) concentration increase, S_0 jumps to 0.60. A further increase in the concentration of wt20 does not increase the S_0 of DPPTC significantly. The curve of S_0 of DPPTC at 37°C shows exactly the same pattern as that at 25°C (Fig. 2). By contrast, as ΔG1 is added at either temperature, the S_0 of DPPTC in DMPC remains constant within experimental error over the whole range of concentration of ΔG1 studied. At pH 7, the S_0 of DPPTC in DMPC increases with the concentration of wt20 at 25°C and 37°C, in a similar manner to that at pH 5, but there is a smaller jump in S_0 of 0.2 at a wt20 concentration of 1.5×10^{-3}, showing that the increase in ordering of DPPTC in DMPC upon binding of wt20 is pH-dependent. Again, at pH 7 as ΔG1 is added, the S_0 of DPPTC in DMPC remains unchanged at both temperatures.

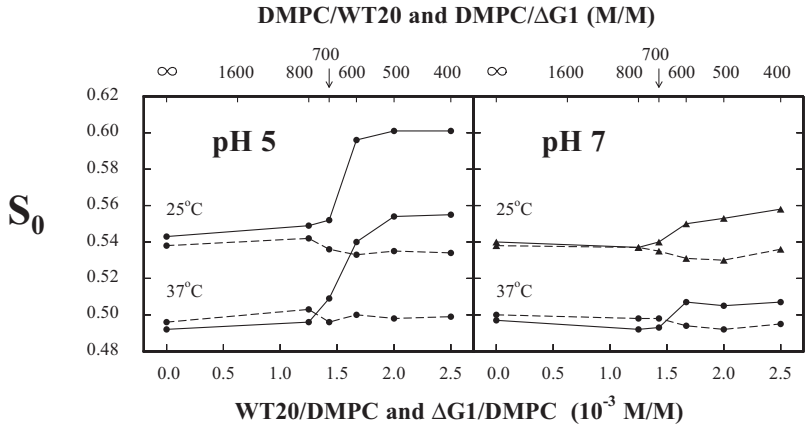

FIGURE 2 Plot of order parameter S_0 of DPPTC in DMPC versus concentration of wt20 (*solid line*) and ΔG1 (*dashed line*) in DMPC dispersions at 25°C and 37°C for conditions of pH 5 and pH 7.

The S_0 of DPPTC in POPC versus wt20 (*solid lines*) and ΔG1 (*dashed lines*) concentrations for both values of pH is plotted in Fig. 3 for 25°C and 37°C. The results are quite similar to those in Fig. 2, but with some differences. Again, a sharp increase occurs in S_0 at pH 5, but of a smaller magnitude (0.2 to 0.3), and it occurs at a slightly higher concentration of wt20, of 2.0×10^{-3}. At pH 7, the binding of wt20 to the POPC bilayer has no significant effect on the S_0 of DPPTC. In all cases, the results with ΔG1 remain constant as the ΔG1/POPC ratio is varied. These comparisons suggest that the pH-dependent headgroup ordering effect of wt20 may be common for all PC bilayers, but its magnitude may depend on the structure of individual PCs.

Before these studies of the interactions of the fusion peptide with bilayers, we carefully characterized the dynamic structure of DMPC bilayers as viewed by ESR spectroscopy, (results not shown). The NLLS spectral simulations show that as the temperature decreases from above to below 23.3°C, changes in the $R_\perp$, $R_\parallel$, and S_0 of the spin labels DPP-Tempo, 5PC, and 14PC are typical of passing through the main phase transition. The changes in dynamic order parameters of DPP-Tempo from above to below 23.3°C show characteristics similar to those we previously observed for the main phase transition of DOPC bilayers (33). These results indicate that DMPC bilayers undergo their main phase transition near 23.3°C. This is a little lower than the main phase transition temperature of pure DMPC (23.9°C), which we attribute to the presence of the spin label in DMPC bilayers. Our ESR observations also confirm that at 25°C, the phase transition exerts no significant effects on the ordering of DMPC bilayers. Furthermore, the ordering effect of wt20 on the headgroups in DMPC and POPC bilayers is very similar at 25°C and 37°C, as we have already indicated.

To supplement the results obtained from the spin-label DPPTC, we studied the binding of wt20 and ΔG1 to DMPC bilayers, using another spin-label DPP-Tempo with a headgroup structure different from that of DPPTC (Fig. 1). We compared binding at pH 5 and pH 7, using a single temperature, given that the ordering effect of wt20 for the headgroup was found to be nearly temperature-independent, according to our study with DPPTC. The binding results measured from DPP-Tempo are given in Fig. 4. It is evident that at a molar ratio wt20/DMPC of 1.5×10^{-3}, there is a sharp increase in the S_0 of DPP-Tempo of 0.5 at pH 5, and a much smaller increase of 0.1 at pH 7. However, S_0 is constant when ΔG1 is used. These features are virtually the same as those shown in Fig. 2, except that the S_0 of

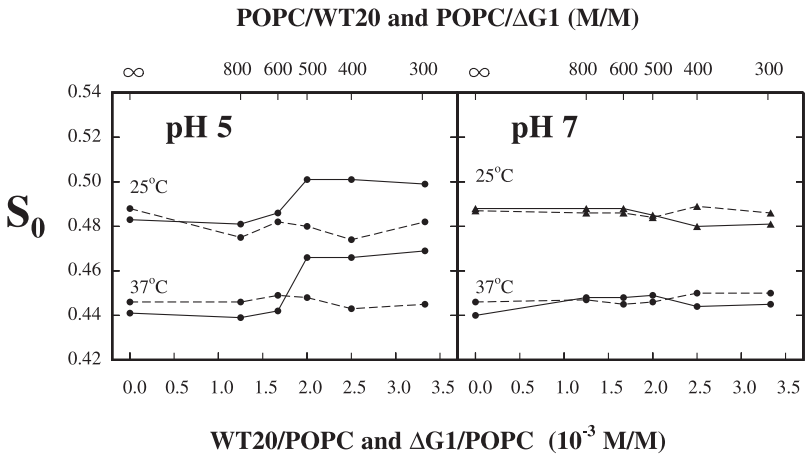

FIGURE 3 Plot of order parameter S_0 of DPPTC in POPC versus concentration of wt20 (*solid line*) and ΔG1 (*dashed line*) in POPC dispersions at 25°C and 37°C for conditions of pH 5 and pH 7.

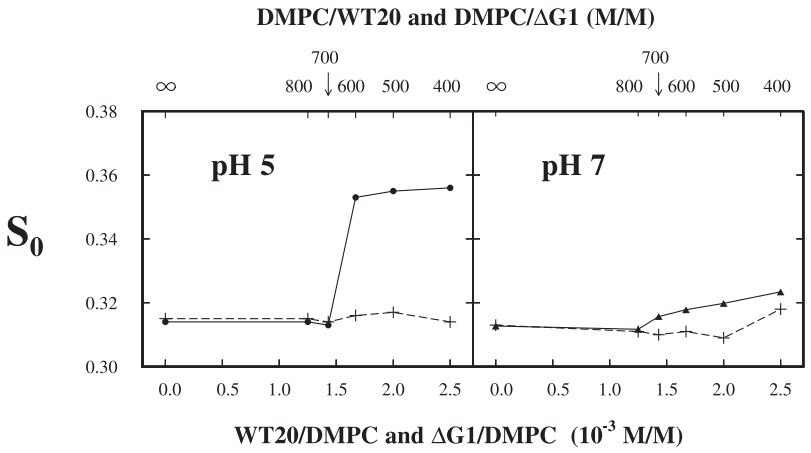

FIGURE 4 Plot of order parameter S_0 of DPP-Tempo in DMPC versus concentration of wt20 (*solid line*) and ΔG1 (*dashed line*) in DMPC dispersions at 25°C for conditions of pH 5 and pH 7.

DPPTC in pure DMPC at 25°C is 0.54, which is much larger than that of DPP-Tempo in DMPC at 25°C, i.e., 0.32. We suggest the following explanation for the difference: the phosphoryl-Tempo-choline group in DPPTC is zwitterionic, but the phosphoryl-Tempo group (without choline) in DPP-Tempo is not ionic. Thus, the dipolar interaction between the phosphoryl-Tempo-choline group in DPPTC and the surrounding headgroups in DMPC is stronger than the interaction between the phosphoryl-Tempo group in DPP-Tempo and the surrounding headgroups in DMPC, implying greater orienting forces seen by the phosphoryl-Tempo-choline group in DPPTC. The significance of orienting forces will be discussed further.

Thus, we confirm that: 1), binding of wt20 significantly increases the order in the headgroup region of DMPC bilayers; 2), this headgroup-ordering effect is stronger at pH 5 than at pH 7; and 3), the nonfusogenic mutant ΔG1 has no such effect.

We also studied the effect of the binding of wt20 and ΔG1 on the ordering of the acyl chains in DMPC bilayers, using chain spin labels 5PC and 14PC at pH 5 and pH 7. The results obtained using 5PC are plotted in Fig. 5, which shows a very similar pattern for the curves of S_0 versus the concentration of wt20 seen for the headgroup probes. Thus, the value of S_0 of 5PC in DMPC jumps from ~0.38 to 0.41–0.42 at pH 5, but jumps from 0.39 to 0.41 at pH 7, a smaller change in S_0, as the concentration of wt20 reaches 1.7×10^{-3}. Again, the S_0 values of 5PC do not vary with concentration of ΔG1. The results of binding experiments using 14PC are plotted in Fig. 6. Evidently, the effect of wt20 on the ordering of 14PC in DMPC is almost negligible, as is the binding of ΔG1 under both pH conditions. These results show that the increase in ordering is strongest in the headgroup region, but it vanishes near the end of the acyl chain.

The sharp increase in S_0 of DPPTC, DPP-Tempo, and 5PC at a precise concentration of wt20 in DMPC and POPC vesicles indicates that wt20 interacts with the DMPC and POPC bilayers in a cooperative fashion. Han and Tamm (41) reported that the HA2 fusion peptide reversibly self-associated into β-sheets on the bilayer surface of POPC/POPG small unilamellar vesicles when the concentration of fusion peptide exceeded a critical value ranging from 1–5 peptides per 1000 lipids, which was interpreted in terms of cooperative binding of the fusion peptide. We suggest that the ordering effect we observed in the MLVs is associated with the interaction between wt20 and the surface of DMPC MLVs, which is likely similar to the interaction of fusion peptide with the surface of small unilamellar vesicles

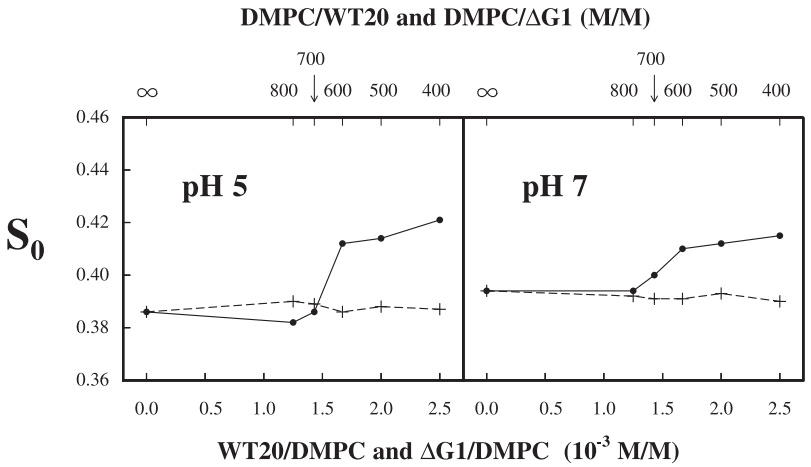

FIGURE 5 Plot of order parameter S_0 of 5PC in DMPC versus concentration of wt20 (*solid line*) and ΔG1 (*dashed line*) in DMPC dispersions at 25°C for conditions of pH 5 and pH 7.

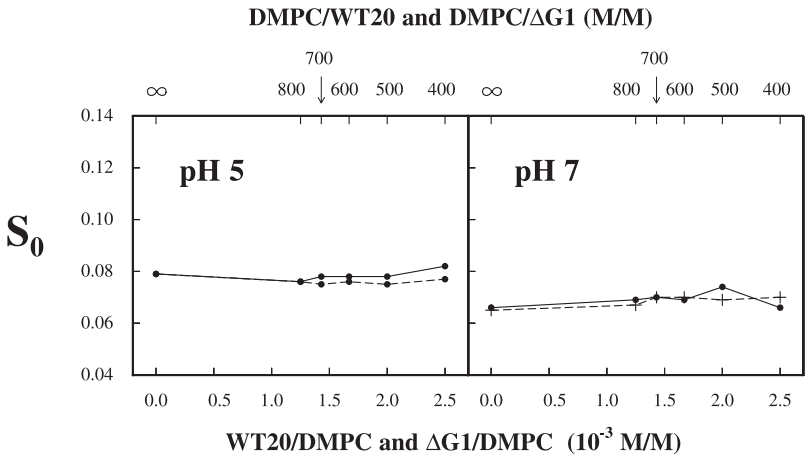

FIGURE 6 Plot of order parameter S_0 of 14PC in DMPC versus concentration of wt20 (*solid line*) and ΔG1 (*dashed line*) in DMPC dispersions at 25°C for conditions of pH 5 and pH 7.

of POPC/POPG observed by Han and Tamm (41). Our ESR results with MLVs should then involve a superposition of spectra from spin labels in the outer leaflet that are significantly affected by the insertion of the peptide and spin labels in the interior, which are not. Given the smaller fraction of the former, this could be manifested as a single ''average'' spectrum from which both components are not resolved. For example, consider that the observed S_0 of the spectrum of DPPTC in DMPC with a DMPC/wt20 of 600 is 0.60. However, this spectrum can be well-constructed by the superimposition of two spectra, with S_0 values of 0.69 and 0.54, with relative populations of 10% and 90%, respectively.

The best-fit values of $R_\perp$, $R_\parallel$, and S_0 obtained from NLLS analyses for DPP-Tempo, 5PC, and 14PC in DMPC, and for DPPTC in DMPC and POPC, versus concentrations of wt20 and ΔG1 at pH 5 and pH 7 are listed in Tables S1–S28 in the Supporting Material. These data show that the binding of wt20 and ΔG1 to DMPC and POPC bilayers does not affect the rotational diffusion rates of the headgroups or acyl chains significantly. Because S_2 values are much smaller (and hence much less accurate) than their corresponding S_0 values for all spin labels and show no distinctive patterns, they are not given in Tables S1–S28 in the Supporting Material.

The lipid composition in bilayers is known to affect membrane fusion. For example, the incorporation of lyso-PC into the outer leaflet of bilayers inhibits membrane fusion (42–45), whereas the incorporation of AA into the outer leaflet of bilayers promotes membrane fusion (44). To explore whether these effects are related to changes in headgroup ordering, we measured the variation of S_0 of DPP-Tempo in DMPC after 1-palmitoyl-2-hydroxyl-PC and AA were added to DMPC bilayers. Indeed, as shown in Fig. S1, at pH 7 and at 25°C, the S_0 of DPP-Tempo decreased from 0.31 for pure DMPC to 0.25 after 10 mol % of 1-palmitoyl-2-hydroxyl-PC were added to DMPC bilayers. Also, as shown in Fig. S2, at pH 7 and at 25°C, the S_0 of DPP-Tempo increased steadily from 0.32 to 0.34, as 10 mol % of AA were added to DMPC bilayers. These results suggest that increasing (or decreasing) the headgroup ordering by altering bilayer lipid composition may be associated with changes in the bilayer structure that may affect membrane fusion.

The best-fit parameters from NLLS analyses of $R_\perp$, $R_\parallel$, and S_0 for DPP-Tempo, varying with concentrations of lyso-PC and AA, are listed in Table S29 and Table S30, respectively.

DISCUSSION

We found that binding of the wild-type HA2 fusion peptide wt20 to DMPC and POPC bilayers mainly increases the ordering of headgroups. These increases are stronger at pH 5 than at pH 7. However, binding of the fusion-inactive mutant ΔG1 does not increase the order of PC bilayers at either pH. These results are consistent with observations that the more fusogenic HA2 fusion peptides increase membrane-ordering more strongly than do the less fusogenic mutants (28,29). Moreover, these results can be correlated with those of a micropipette aspiration study, i.e., that swelling and lysis of SOPC vesicles were induced upon wt20 binding, and more strongly at pH 5 than at pH 7, whereas no swelling was evident upon ΔG1 binding (4).

Our results may appear inconsistent with those of the molecular-dynamic simulations (20–22) described in the Introduction. This can be readily explained. We found that an increase in membrane ordering is a cooperative effect of wt20 on bilayer structure, requiring a well-defined concentration of wt20. Molecular-dynamics simulations explore how a single fusion peptide interacts with the bilayers. Thus, only the local perturbation of the bilayer by the fusion peptide was observed, and not the cooperative effect of fusion peptide binding. In addition, we found that the membrane-fusion inhibitor 1-palmitoyl-2-hydroxyl-PC decreased, whereas the membrane-fusion promoter AA increased, the headgroup ordering of DMPC bilayers. These correlations suggest that increases in headgroup ordering may cause changes in bilayer structure that are important for membrane fusion.

Significance of the order parameter, S_0

The order parameter S_0 represents the axial ordering of lipid molecules in bilayers, which originates from the lateral restoring (aligning) torques $L(\theta)$ exerted on each lipid molecule from its neighboring lipid molecules. Here, θ is the angle between the primary axis for a chain segment or a headgroup and the normal to the bilayer, with $\theta = 0$ as the preferential orientation of lipid molecules. These restoring torques are associated with an orienting potential $U(\theta)$ in the bilayer, which is related to $L(\theta)$ by $dU(\theta)/d\theta = -L(\theta)$, and is minimized when θ equals zero. In NLLS analyses, S_0 was calculated according to the best-fit value of $U(\theta)$. Thus S_0 is a measure of lateral cohesive forces between lipid molecules in the lipid bilayer, and it indicates how strongly a chain segment or headgroup is aligned along the normal to the lipid bilayer. An increase in S_0 in the acyl-chain region or headgroup region indicates that the lateral packing density in that region is increased, or that the local region becomes more condensed and more solid-like. Molecular interactions between lipid molecules are dominated by van der Waals forces in the acyl-chain region, but are primarily ionic (generated by hydrogen bonding) in the headgroup region. Because the strengths of hydrogen bonds, ranging from 10–40 kJ mol^{-1}, are much stronger than those of a typical van der Waals ''bond'' (~1 kJ mol^{-1}) (46), changes in the S_0 of headgroups would affect the bilayer structure more significantly than changes in the S_0 of acyl chains, as we shall discuss.

The restoring torque is related to, but different from, the lateral pressure that is frequently cited (47–49). For example, the restoring torque is a microscopic molecular quantity, whereas the lateral pressure is a macroscopic membrane force that is similar to the stress in bilayers.

Condensation of the outer leaflet induces bending moment in the bilayer

The ordering effect of wt20 can alter the bilayer structure in a vesicle. Because the ratio of the radius of the vesicle to the thickness of the bilayer in a LUV or a giant unilamellar vesicle is large, the mechanical equilibrium in a vesicle can be approximately described in terms of stresses and pressures exerted on the outer and inner surfaces of vesicles (50). However, if relative deformations of two leaflets occur, even if they are small, large bending stresses could be generated in the bilayer because of coupling between the two leaflets (51). This is likely the case for the binding of wt20 to a vesicle, as described below.

When wt20 is added to a unilamellar vesicle solution at pH 5, it binds to the outer leaflet of the vesicle bilayers, and increases the S_0 of the headgroup and of the acyl chain near the headgroup in the outer leaflet of the bilayers. The outer layer becomes more condensed and more solid-like, which tends to shrink its area. Because two monolayers in a closed vesicle cannot slide relative to each other, they are effectively mechanically coupled (51). This means that the tendency toward shrinkage in the condensed outer layer will generate a compressive force exerted on the inner layer, tending to reduce the area of the inner layer. But this is resisted by the inner layer, which remains softer. Thus, the inner layer would exert a counterstretching force on the outer layer. It follows that the condensed outer layer experiences a stretching stress, whereas the soft inner layer is under a compressive stress. Thus a nonuniform distribution of stress across the bilayer is created. Therefore, a bending moment in the bilayer would be generated (51), which tends to bend the vesicle bilayer toward the outer surface of the vesicle.

The bending moment in a bilayer is given by $\int_{-t}^{t} T(z)z dz$, where $T(z)$ is a profile of the stress across the bilayer, z is the distance of the tangent plane of the lateral stress from the middle surface of the bilayer, and $2t$ is the thickness of the bilayer. Let us consider this integral for the wt20-induced bending moment: 1), Bending rigidity increases significantly when a bilayer is condensed, and it is harder to stretch a condensed bilayer than to stretch a bilayer in the fluid state. 2), Ionic interactions in the headgroup region are much stronger than the van der Waals interactions in the acyl-chain region. 3), The increase in S_0 for the headgroups is larger than that for the acyl chains upon binding of wt20 (see Results). 4), Values of z in the integral corresponding to the headgroup region are larger than those corresponding to the acyl-chain region. In sum, terms from the stretching forces in the headgroup region make a larger contribution to the integral than those from the acyl-chain region. Thus the bending moment in a vesicle bilayer is largely generated by the increased ordering of headgroups in the outer leaflet.

An increase in the ordering of headgroups is known to be correlated with the dehydration of headgroups (33,52,53). The importance of membrane-surface dehydration for membrane fusion has long been appreciated (28,54,55). Membrane dehydration involves changes in the chemical bonding structure in the headgroup region that strengthen the hydrogen bonds in the headgroup region (56). Thus, the wt20-induced bending moment belongs to a type of ''chemically induced moment'' in bilayers, a term introduced by Evans (57) for bending moments in bilayers that are produced by changes in the chemical environment of bilayer surroundings (51).

How do wt20-induced bilayer bending moments affect membrane fusion?

Bending stresses induced by wt20 binding tend to bend the bilayer toward the outer surface of the vesicle, i.e., to increase the negative curvature of the vesicle bilayer. How does this bilayer curvature change affect membrane fusion? A suggested membrane-fusion pathway (58) can be briefly described as follows. After contact between two apposing bilayers, an intermediate membrane structure, called a stalk,

is formed by the merging of contacting leaflets of the two bilayers. The stalk will evolve, possibly through hemifusion, into an initial fusion pore, which may flicker (close and open repeatedly). The fusion pore will be enlarged by stresses in the bilayers as a result of vesicle swelling. This stalk-fusion-pore hypothesis lies at the heart of the widely accepted model of membrane fusion, but its mechanism remains largely unknown. Based on observations that both the fusion peptide and transmembrane domain in HA dehydrate bilayers, Han et al. (28) suggested that dehydration on the surfaces of the cell plasma membrane and viral membrane might be a prerequisite for viral fusion. Because membrane-surface dehydration promotes negative curvature of the membrane, we propose that bending moments generated in both cell and viral membranes would promote stalk formation in the early stage of fusion. Our suggestion is supported by a recent mutation study of the fusion activity of paramyxovirus parainfluenza virus 5 (PIV5): two residues in the transmembrane domain of the F protein from PIV5 were identified as crucial for the merging of cell and viral membranes. This function was ascribed to the role of the two residues in facilitating the negative curvature of the viral membrane (59).

The negative-curvature-promoting bending moments also play a role in the late stage of fusion. Fused vesicles and cells were reported to grow from a dumbbell shape to a spherical shape (60,61). Because the ratio of volume/surface area for a spherical vesicle increases with the size of the vesicle, this shape change is accompanied by an increase in the enclosed aqueous volume in the fused vesicle, i.e., by swelling. Thus, after enlargement of the fusion pore, vesicle-swelling continues through the completion of fusion. We propose that the shape change, as dominated by the expansion (i.e., an increase in negative curvature) of the two balls in the dumbbell, is aided by the bending moments.

Electrostatic free energy is released because of enhanced dipolar interactions

Because the ordering of headgroups and the ordering of bilayer surface water are correlated (33,62), the binding of wt20 also increases the ordering of water on the outer surface of vesicles. When the headgroup region becomes more ordered, dipolar interactions in the headgroup region are enhanced and the electrostatic energy is lowered, i.e., becomes more negative in its value. We suggest that the lowered electrostatic energy may make a significant contribution to the overall reduction in free energy upon fusion peptide binding to the bilayer.

The increased ordering of both headgroups and water molecules indicates that the headgroup region is more strongly polarized along the direction normal to the bilayer. This would result in an increase in membrane-surface dipole potential, which mainly originates from ordered membrane-surface water molecules (63). Indeed, the activity of simian immunodeficiency virus-mediated membrane fusion was reported to be correlated with the measured dipole potential of the membrane (64).

Lipid transverse asymmetry induces an asymmetric change in bilayer ordering

Here we consider the effects on membrane fusion of the asymmetric incorporation of lyso-PC and AA into a bilayer. We showed that 1-palmitoyl-2-hydroxyl PC reduces headgroup ordering in DMPC bilayers. This is consistent with a report that the apparent area-expansion modulus of egg-PC bilayers was reduced after the incorporation of lyso-PC, indicating that lyso-PC softens egg-PC bilayers (65). Softening of the headgroup region in the outer leaflet of the vesicle bilayer, while the inner leaflet remains unchanged, would generate bending moments with an opposite sign to those after the binding of wt20. Thus the incorporation of lyso-PC into the outer leaflet of a vesicle bilayer would increase the positive curvature of the bilayer, posing an obstacle for stalk formation and vesicle swelling, and inhibiting membrane fusion. Because AA increases the ordering of DMPC headgroups, the incorporation of AA into the outer leaflet of cell membranes has the same effect as the binding of wt20 on the bilayer structure, such that AA is a promoter of membrane fusion.

When lyso-PC was added to the inner leaflet of the bilayer, influenza HA-mediated cell fusion (66) and poly(ethylene glycerol) (PEG)-induced fusion of DPPC LUV (67) were reportedly promoted. Assuming that lyso-PC is incorporated into the inner leaflet of the cell membrane, it will reduce the ordering of the headgroups in the inner leaflet of the cell membrane. This change will create consequences similar to what we described in the case of the binding of wt20 to vesicles: compressive forces in the inner leaflet of the cell membrane and stretching forces in the outer leaflet of the cell membrane will be generated. This would also result in bending moments that tend to increase the negative curvature of the cell membrane. This may explain why the addition of lyso-PC in the inner leaflet of the cell membrane promotes HA-mediated cell fusion.

The regulatory role of the membrane fusion of lyso-PC was initially attributed to its inverted-cone molecular shape, which would affect lipid packing in the two leaflets differently, and affecting the curvature of the bilayer in opposite ways if lyso-PC were added to the inner versus outer leaflet of the bilayer (66). However, after analyzing the effect of the asymmetric transverse distribution of lyso-PC (67) and the effect of altering the molecular shape of cardiolipin on PEG-mediated vesicle fusion, Lee and Lentz (68) concluded that outer-leaflet packing disruption is necessary to induce fusion, and molecular shape plays no role in PEG-mediated vesicle fusion. Moreover, in the calcium phosphate-induced fusion of human erythrocytes, the Ca^{2+} threshold of fusion was reported to be significantly lowered after

phosphatidyleserine was exposed on the surface of the plasma membranes, or after incorporation of spin-labeled PS into the outer leaflet of the cell (69). This result cannot be interpreted in terms of the cylindrical shape of the PS molecule, but can be understood in terms of the increased negative curvature of the bilayer induced by the outer leaflet hardening because of the dehydrating effect of Ca^{2+} on PS headgroups (70), when PS is exposed to the outer surface of the bilayer. Molecular shape appears unlikely to be a major factor in affecting membrane-fusion activity.

The cooperative aspect of the bilayer surface-ordering effect of wt20 that we observed is likely related to the surface self-association of wt20 (41). This is consistent with observations to the effect that the oligomerization of HA fusion peptide enhances peptide-induced lipid mixing and vesicle leakage (71), and that the clustering of dengue-virus fusion peptide on the bilayer surface leads to deeper insertion of the peptide into the bilayer (72). The self-aggregation of HA fusion peptide on the bilayer surface may indicate that cooperative interactions of HA with the cell membrane are required for HA-mediated membrane fusion (73).

Bending stresses induced by the ''half-hardening'' of the bilayer provide a mechanism for curving the bilayers, in addition to the proposed protein scaffolding mechanism (74–76) and the lipid-packing perturbation mechanism (i.e., the insertion of protein into the outer leaflet, behaving like a wedge, and perturbing the lipid packing) (74,77). Specialized proteins and protein/protein interactions are required for various membrane structural transformations, such as membrane fusion and fission. Do lipids have only ''a permissive role in membrane curvature'' (77)? Our results indicate that changes induced in the membrane structure because of alterations in lipid composition and lipid/protein interactions have a significant effect on membrane curvature, suggesting that bilayer structural changes may play an active role in biological membrane remodeling.

CONCLUSIONS

The major effect that we found of wt20 binding to DMPC and POPC bilayers was to increase the order of headgroups at a critical concentration of wt20. This effect was stronger at pH 5 than at pH 7. However, the binding of ΔG1 to DMPC and POPC bilayers had no such effect on the ordering of bilayers. We suggest that coupling between the condensed outer leaflet and softer inner leaflet upon wt20 binding generates bending stresses in the vesicle bilayer, increasing the negative curvature of the vesicle bilayer. This change in bilayer curvature may promote stalk formation and assist vesicle-swelling during the late stage of fusion.

SUPPORTING MATERIAL

Thirty-one tables and two figures are available at http://www.biophysj.org/biophysj/supplemental/S0006-3495(09)00802-9.

We thank Ms. Qi Wang for her initial work in this study, and Drs. Boris Dzikovski and Peter Borbat for helpful discussions.

This work was supported by National Institutes of Health/National Institute of Biomedical Imaging and BioEngineering grant EB03150 and National Institutes of Health/National Center for Research Resources grant P41-RR 016292.

REFERENCES

1. Martens, S., and McMahon. 2008. Mechanisms of membrane fusion: disparate players and common principles. *Nat. Rev. Mol. Cell Biol.* 9:543–556.
2. White, J. M., S. E. Delos, M. Brecher, and K. Schornberg. 2008. Structures and mechanisms of viral membrane fusion proteins: multiple variations on a common theme. *Crit. Rev. Biochem. Mol. Biol.* 43:189–219.
3. Shangguan, T., D. Alford, and J. Bentz. 1996. Influenza virus-liposome lipid mixing is leaky and largely insensitive to the material properties of the target membrane. *Biochemistry.* 35:4956–4965.
4. Longo, M. L., A. J. Waring, and D. A. Hammer. 1997. Interaction of the influenza hemagglutinin fusion peptide with lipid bilayer: area expansion and permeation. *Biophys. J.* 73:1430–1439.
5. Cheng, S. F., C. W. Wu, E. A. Kantchev, and D. K. Chang. 2004. Structure and membrane interaction of the internal fusion peptide of avian sarcoma leucosis virus. *Eur. J. Biochem.* 274:4725–4736.
6. Duzqunes, N., and S. A. Shavnin. 1992. Membrane destabilization by N-terminal peptides of viral envelope proteins. *J. Membr. Biol.* 128:71–80.
7. Haque, M. E., A. J. McCov, J. Glenn, J. Lee, and B. R. Lentz. 2001. Effects of hemagglutinin fusion peptide on poly(ethylene glycol)-mediated fusion of phosphatidylcholine vesicles. *Biochemistry.* 40:14243–14251.
8. Zhelev, D. V., N. Stoicheva, P. Scherrer, and D. Needham. 2001. Interaction of synthetic HA2 influenza fusion peptide analog with model membranes. *Biophys. J.* 81:285–304.
9. Perez-Bema, A. J., J. Guillen, M. R. Moreno, A. I. Gomez-Sanchez, G. Pabst, et al. 2008. Interaction of the most membranotropic region of the HCV E2 envelope glycoprotein with membrane. Biophysical characterization. *Biophys. J.* 94:4737–4750.
10. Li, Y., and L. K. Tamm. 2007. Structure and plasticity of the human immunodeficiency virus gp41 fusion domain in lipid micelles and bilayers. *Biophys. J.* 93:876–885.
11. Macosko, J. C., C. H. Kim, and Y.-K. Shin. 1997. The membrane topology of fusion peptide region of influenza hemagglutinin determined by spin-labeling EPR. *J. Mol. Biol.* 267:1139–1148.
12. Wharton, S. A., S. R. Martin, R. W. H. Ruigrok, J. J. Skehel, and D. C. Wiley. 1988. Membrane fusion by peptide analogs of influenza virus haemagglutinin. *J. Gen. Virol.* 69:1847–1857.
13. Kim, C.-H., J. C. Macosko, and Y.-K. Shin. 1998. The mechanism for low-pH induced clustering of phospholipid vesicles carrying the HA2 ectodomain of influenza hemagglutinin. *Biochemistry.* 37:137–144.
14. Han, X., J. H. Bushweller, D. S. Cafiso, and L. K. Tamm. 2001. Membrane structure and fusion-triggering conformational change of the fusion domain from influenza hemagglutinin. *Nat. Struct. Biol.* 8:715–720.
15. Hsu, C.-H., S. H. Wu, D. K. Chang, and C. Chen. 2002. Structural characterization of fusion peptide analogs of influenza virus hemagglutinin. Implication of the necessity of a helix-helix motif in fusion activity. *J. Biol. Chem.* 277:22725–22733.
16. Guillen, J., A. J. Perez-Berna, M. R. Moreno, and J. Villalain. 2008. A second SARS-CoV S2 glycoprotein internal membrane-active peptide. Biophysical characterization and membrane interaction. *Biochemistry.* 47:8214–8224.
17. Sammalkorpi, M., and T. Lazaridis. 2007. Configuration of influenza hemagglutinin fusion peptide monomers and oligomers in membranes. *Biochim. Biophys. Acta.* 1768:30–38.

18. Esbjorner, E. K., K. Oglecka, P. Lincoln, A. Graslund, and B. Norden. 2007. Membrane binding of pH-sensitive influenza fusion peptides. Positioning, configuration, and induced leakage in a lipid vesicle model. *Biochemistry*. 46:13490–13504.

19. Castano, S., and B. Desbat. 2005. Structure and orientation study of fusion peptide FP23 of gp41 from HIV-1 alone or inserted into various lipid membrane models (mono-, bi- and multibi-layers) by FT-IR spectroscopies and Brewster angle microscopy. *Biochim. Biophys. Acta*. 1715:81–95.

20. Lague, P., B. Roux, and R. W. Pastor. 2005. Molecular dynamics simulations of the influenza hemagglutinin fusion peptide in micelles and bilayers: conformational analysis of peptide and lipids. *J. Mol. Biol.* 354:1129–1141.

21. Vaccaro, L., K. J. Cross, J. Kleinjung, S. K. Straus, D. J. Thomas, et al. 2005. Plasticity of influenza hemagglutinin fusion peptides and their interaction with lipid bilayers. *Biophys. J.* 88:25–36.

22. Volnsky, P. E., A. A. Polyansky, N. A. Simakov, A. S. Arseniev, and R. G. Efremov. 2005. Effect of lipid composition on the ''membrane response'' induced by a fusion peptide. *Biochemistry*. 44:14626–14637.

23. LeDuc, D. L., Y.-K. Shin, R. F. Epand, and R. M. Epand. 2000. Factors determining vesicular lipid mixing induced by shortened constructs of influenza hemagglutinin. *Biochemistry*. 39:2733–2739.

24. Tristran-Nagle, S., and J. F. Nagle. 2007. HIV-1 fusion peptide decreases bending energy and promotes curved fusion intermediates. *Biophys. J.* 93:2048–2055.

25. Haque, M. E., V. Koppaka, P. H. Axelsen, and B. R. Lentz. 2005. Properties and structures of the influenza and HIV fusion peptides on lipid membranes: implications for a role in fusion. *Biophys. J.* 89:3183–3194.

26. Aranda, F. J., J. A. Teruel, and A. Ortiz. 2003. Interaction of a synthetic peptide corresponding to the N-terminus of canine distemper virus fusion protein with phospholipids vesicles: a biophysical study. *Biochim. Biophys. Acta*. 1618:51–58.

27. Gray, C., S. A. Tatulian, S. A. Wharton, and L. K. Tamm. 1996. Effect of the N-terminal glycine on the secondary structure, orientation, and interaction of the influenza hemagglutinin fusion peptide with lipid bilayers. *Biophys. J.* 70:2275–2286.

28. Han, X., D. A. Steinhauer, S. A. Wharton, and L. K. Tamm. 1999. Interaction of mutant influenza virus hemagglutinin fusion peptides with lipid bilayers: probing the role of hydrophobic residue size in the central region of the fusion peptide. *Biochemistry*. 38:15052–15059.

29. Wu, C. H., S. F. Chen, W. N. Huang, V. D. Trivedi, B. Veeramuthu, et al. 2003. Effect of alterations of the amino-terminal glycine of influenza hemagglutinin fusion peptide on its structure, organization and membrane interaction. *Biochim. Biophys. Acta*. 1612:41–51.

30. Lai, A. L., and L. K. Tamm. 2007. Locking the kink in the influenza hemagglutinin fusion domain structure. *J. Biol. Chem.* 282:22946–22956.

31. Swamy, M. J., L. Cianti, M. Ge, A. K. Smith, D. Holowka, et al. 2006. Coexisting domains in the plasma membranes of live cells characterized by spin-label spectroscopy. *Biophys. J.* 90:4452–4465.

32. Ge, M., A. Gidwani, H. A. Brown, D. Holowka, B. Baird, et al. 2003. Ordered and disordered phases coexist in plasma membrane vesicles of RBL-2H3 mast cells. An ESR study. *Biophys. J.* 85:1278–1288.

33. Ge, M., and J. H. Freed. 2003. Hydration, structure, and molecular interactions in the headgroup region of dioleoylphospatidylcholine bilayers: an ESR study. *Biophys. J.* 85:4023–4040.

34. Ge, M., and J. H. Freed. 1999. Electron-spin resonance study of aggregation of gramicidin in DPPC bilayers and hydrophobic mismatch. *Biophys. J.* 76:264–280.

35. Ge, M., K. A. Field, R. Aneja, D. Holowka, B. Baird, et al. 1999. Electron spin resonance characterization of liquid ordered phase of detergent membranes from RBL-2H3 cells. *Biophys. J.* 77:925–933.

36. Budil, D. E., S. Lee, S. Saxena, and J. H. Freed. 1996. Nonlinear-least-squares analysis of slow-motion EPR spectra in one and two dimensions using a modified Levenberg-Marquardt algorithm. *J. Magn. Reson. A.* 120:155–189.

37. Steinhauer, D. A., S. A. Wharton, J. J. Skehel, and D. C. Wiley. 1995. Studies of the membrane fusion peptide mutants of influenza virus hemagglutinin. *J. Virol.* 69:6643–6651.

38. Meirovitch, E., D. Igner, G. Moro, and J. H. Freed. 1982. Electron-spin relaxation and ordering in smectic and supercooled nematic liquid crystals. *J. Chem. Phys.* 77:3915–3938.

39. Schneider, D. J., and J. H. Freed. 1989. Calculating slow motional magnetic resonance spectra: a user's guide. *In* Spin Labeling Theory and Applications, Vol. 8 L. J. Berliner and J. Reuben, editors. Plenum Press, New York. 1–76.

40. Meirovitch, E., A. Nayeem, and J. H. Freed. 1984. Analysis of protein-lipid interactions based on model simulations of electron spin resonance spectra. *J. Phys. Chem.* 88:3454–3465.

41. Han, X., and L. K. Tamm. 2000. pH dependent self-association of influenza hemagglutinin fusion peptides in lipid bilayers. *J. Membr. Biol.* 304:953–965.

42. Yeagle, P. L., F. T. Smith, J. E. Young, and T. D. Flanagan. 1994. Inhibition of membrane fusion by lysophosphatidylcholine. *Biochemistry*. 33:1820–1827.

43. Martin, I., and J. M. Ruysschaert. 1995. Lysophosphatidylcholine inhibits vesicles fusion induced by the NH_2-terminal extremity of SIV/HIV fusogenic proteins. *Biochim. Biophys. Acta*. 1240:95–100.

44. Chernomordik, L. V., E. Leikina, M. Cho, and J. Zimmerberg. 1995. Control of baculovirus gp64-induced syncytium formation by membrane lipid composition. *J. Virol.* 69:3049–3058.

45. Ohki, S., G. A. Baker, P. M. Page, T. A. McCarty, R. M. Epand, et al. 2006. Interaction of influenza virus fusion peptide with lipid membranes: effect of lysolipid. *J. Membr. Biol.* 211:191–200.

46. Israelachivili, J. 1991. Intermolecular and Surface Forces, 2nd ed.. Academic Press, New York.

47. Sackmann, E. 1995. Physical basis of self-organization and function of membranes: physics of vesicles in structures and dynamics of membranes. *In* Handbook of Biological Physics, Vol. 1 R. Lipowsky and E. Sackmann, editors. Elsevier Science, New York. 213–304.

48. Janmey, P. A., and P. K. J. Kinnuen. 2006. Biophysical properties of lipids and dynamic membranes. *Trends Cell Biol.* 16:538–546.

49. Marsh, D. 2007. Lateral pressure profile, spontaneous curvature frustration, and the incorporation and conformation of proteins in membranes. *Biophys. J.* 93:3884–3899.

50. Mollmann, H. 1981. Introduction to the Theory of Thin Shell. John Wiley & Sons, Chichester.

51. Evans, E. A., and R. Skalak. 1980. Mechanics and Thermodynamics of Biomembranes. CRC Press, Boca Raton.

52. Binder, H. 2007. Water near lipid membranes as seen by infrared spectroscopy. *Eur. Biophys. J.* 36:265–279.

53. Arnold, K., A. Hermman, K. Gawrisch, and L. Pratsch. 1987. Water-mediated effect of PEG on membrane properties and fusion. *In* Molecular Mechanism of Membrane Fusion. S. Ohki, D. Doyle, T. D. Flanagan, S. W. Hui, and E. Mayhew, editors. Plenum Press, New York. 255–273.

54. Hoekstra, D. 1982. Role of lipid phase separation and membrane hydration in phospholipids vesicle fusion. *Biochemistry*. 21:2833–2840.

55. Wilschut, J., N. Dugunes, and D. Papahadjopoulos. 1981. Calcium/magnesium specificity in membrane fusion: kinetics of aggregation and fusion of phosphatidylcholine vesicles and the role of bilayer curvature. *Biochemistry*. 20:3126–3133.

56. Boggs, J. M. 1987. Lipid intermolecular hydrogen bonding: influence on structural organization and membrane function. *Biochim. Biophys. Acta*. 906:353–404.

57. Evans, E. A. 1974. Bending resistance and chemically induced moments in membrane bilayers. *Biophys. J.* 14:923–931.

58. Zimmerberg, J., and L. V. Chernomordik. 1999. Membrane fusion. *Adv. Drug Deliv. Rev.* 38:197–205.

59. Bissonnete, M. L. Z., J. E. Donald, W. F. DeGrado, T. S. Jardetzky, and R. A. Lamb. 2009. Functional analysis of the transmembrane domain in

paramyxovirus F protein-mediated membrane fusion. *J. Mol. Biol.* 386:14–36.

60. Nomura, F., T. Inaba, S. Ishikawa, M. Nagata, S. Takahashi, et al. 2004. Microscopic observations reveal that fusogenic peptides induce liposome shrinkage prior to membrane fusion. *Proc. Natl. Acad. Sci. USA.* 101:3420–3425.
61. Knutton, S., and T. Bachi. 1980. The role of cell swelling and haemolysis in Sendai virus-induced cell fusion and in the diffusion of incorporated viral antigen. *J. Cell Sci.* 42:153–167.
62. Chen, J., S. Pautot, D. A. Weitz, and X. S. Xie. 2003. Ordering of water molecules between phospholipids bilayers visualized by coherent anti-Stokes Raman scattering microscopy. *Proc. Natl. Acad. Sci. USA.* 100:9826–9830.
63. Gawrisch, K., D. Ruston, J. Zimmerberg, V. A. Parsegian, R. P. Rand, et al. 1992. Membrane dipole potentials, hydration force, and ordering of water at membrane surfaces. *Biophys. J.* 61:1213–1223.
64. Cladera, J., I. Martin, J.-M. Ruysschaert, and P. O'Shea. 1999. Characterization of the sequence of interactions of the fusion domain of the simian immunodeficiency virus with membranes. *J. Biol. Chem.* 274:29951–29959.
65. Zhelev, D. V. 1998. Material property characteristics for lipid bilayers containing lysolipid. *Biophys. J.* 75:321–330.
66. Bailey, A., M. Zhukovsky, A. Glozzi, and L. V. Chernomordik. 2005. Liposome composition effects on lipid mixing between cells expressing influenza virus hemagglutinin and bound liposomes. *Arch. Biochem. Biophys.* 439:211–221.
67. Wu, H., L. Zheng, and B. R. Lentz. 1996. A slight asymmetry in the transbilayer distribution of lysophosphatidylcholine alters the surface properties and poly(ethylene glycerol)-mediated fusion of dipalmitoylphosphatidylcholine large unilamellar vesicles. *Biochemistry.* 35: 12602–12611.
68. Lee, J., and B. R. Lentz. 1997. Outer leaflet-packing defects promote poly(ethylene glycol)-mediated fusion of large unilamellar vesicles. *Biochemistry.* 36:421–431.
69. Schewe, M., P. Muller, T. Korte, and A. Herrmann. 1992. The role of phospholipids asymmetry in calcium-phosphate-induced fusion of human erythrocyte. *J. Biol. Chem.* 267:5910–5915.
70. Dluhy, R. A., D. G. Cameron, H. H. Mantsch, and R. Mendelson. 1983. Fourier transform infrared spectroscopic studies of the effect of calcium ions on phosphatidylserine. *Biochemistry.* 22:6318–6325.
71. Lau, W. L., D. S. Ege, J. D. Lear, D. A. Hammer, and W. F. DeGrado. 2004. Oligomerization of fusogenic peptide promotes membrane fusion by enhancing membrane destabilization. *Biophys. J.* 86:272–284.
72. Stauffer, F., M. N. Melo, F. A. Carneiro, F. J. R. Sousa, M. A. Juliano, et al. 2008. Interaction between dengue virus fusion peptide and lipid bilayers depends on peptide clustering. *Mol. Membr. Biol.* 25:128–138.
73. Danieli, T., S. L. Pelletier, Y. I. Henis, and J. M. White. 1996. Membrane fusion mediated by the influenza hemagglutinin requires the concerted action of at least three hemagglutinin trimers. *J. Cell Biol.* 133:559–569.
74. McMahon, H. T., and J. L. Gallop. 2005. Membrane curvature and mechanisms of dynamic cell membrane remodeling. *Nature.* 438:590–596.
75. Zimmerberg, J., and M. M. Kozlov. 2006. How proteins produce cellular membrane curvature. *Nat. Rev. Mol. Cell Biol.* 7:9–19.
76. Frost, A., R. Perera, A. Roux, K. Spasov, O. Destaing, et al. 2008. Structural basis of membrane invagination by F-BAR domains. *Cell.* 132:807–817.
77. Gallop, J. L., C. C. Jao, H. M. Kent, P. J. B. Bulter, P. R. Evans, et al. 2006. Mechanism of endophilin N-BAR domain-mediated membrane curvature. *EMBO J.* 25:2898–2910.